energies

MDPI

Article

Generic Analysis Framework for Modular Multilevel Converter HVDC with Multi-Infeed Line-Commutated Converter HVDC System

Sehyun Kim [1], Kyeon Hur [2], Jongseo Na [2], Jongsu Yoon [3] and Heejin Kim [4,*]

[1] Electricity Technology Group, Samsung Electronics, Suwon-si 16677, Korea; kshgiawm@gmail.com
[2] School of Electrical and Electronic Engineering, Yonsei University, Seoul 03722, Korea; khur@yonsei.ac.kr (K.H.); jongseo529@yonsei.ac.kr (J.N.)
[3] Korea Electric Power Corporation Research Institute (KEPRI), Daejeon 34056, Korea; jongsu.yoon@kepco.co.kr
[4] R&D Center, Pion Electric, Gwangmyeong-si 14348, Korea
* Correspondence: jimmykim07@gmail.com

Abstract: This paper proposes a generic analysis framework for a grid supporting modular multilevel converter (MMC)-high voltage DC (HVDC) in a multi-infeed of line commutated converter (LCC) and MMC (MILM) system. MMC-HVDC can support the grid by compensating for the exact reactive power consumptions within the MMC-HVDC system and the varying power system conditions in the MILM system. Maximum active/reactive power capability (MPQC) curve and PQ loading curve comparison process is introduced to properly design a grid supporting MMC-HVDC. While the MPQC curve presents the maximum PQ range of the MMC-HVDC system based on the submodule capacitance value and the modulation index, the PQ loading curve presents the reactive power requirement from the power system that MMC-HVDC needs to compensate. Finally, the comparison of these two curves yields the proper value of submodule capacitance and the modulation index for sufficiently supporting the MILM system. The proposed framework is validated with detailed PSCAD/EMTDC simulation; it demonstrated that it could be applied to various power system conditions.

Keywords: multi-infeed; MMC-HVDC; PQ capability; reactive power; LCC-HVDC; EMTDC; short circuit capacity; energy storage requirement

Citation: Kim, S.; Hur, K.; Na, J.; Yoon, J.; Kim, H. Generic Analysis Framework for Modular Multilevel Converter HVDC with Multi-Infeed Line-Commutated Converter HVDC System. *Energies* **2022**, *15*, 184. https://doi.org/10.3390/en15010184

Academic Editors: Georgios Konstantinou, Teuvo Suntio and Miguel Castilla

Received: 24 September 2021
Accepted: 23 December 2021
Published: 28 December 2021

1. Introduction

The line-commutated converter (LCC)-high voltage DC (HVDC) has long been adopted in the power grids and demonstrated to be the preferred solution for several different applications [1–5]. The voltage source converter (VSC)-HVDC technology appeared in 1997 has been employed particularly to resolve the inherent weaknesses of the LCC-HVDC [1]. Among the VSC topology options, the modular multilevel converter (MMC) has become the most attractive solution for DC transmission systems; many experts have continuously contributed theoretically to the MMC: the fundamental principles and structure, controls, modeling, internal dynamics, and submodule voltage-balancing methods [6–21]. Practical yet challenging concept planning by building multi-infeed MMC-HVDC with the existing LCC-HVDC system has emerged to reinforce the growing power system, e.g., multi-infeed LCC-HVDC and MMC-HVDC (MILM) in Skagerrak, Denmark, and Jeju HVDC No. 3 under construction in South Korea. The MMC-HVDC actively supports the power system at full capacity with LCC-HVDC under various MILM operating conditions and helps avoid AC/DC interactions. An integration of heavily system-dependent LCC-HVDC and new MMC-HVDC for desired grid support functions require proper analysis to maximize benefits. The understanding of the fundamental components affecting the capability of MMC-HVDC in planning phase enables fast, efficient, and accurate conclusions prior to

the detailed planning phase from the system planner point of view. There have been several useful studies on static analysis for single and multi-infeed of LCC-HVDC that define their operating regions through the maximum power curve (MPC) analysis for a proper integration [22–32]. Furthermore, there have been studies on the design criteria of MMC-HVDC that investigate the internal dynamics and elaborate on the active and reactive power (*PQ*) operating region [33–37]. Moreover, there have been studies on multi-infeed of LCC-HVDC and VSC-HVDC, combining two operating regions into one form, to investigate interactions and proper control the balanced performance [38–43]. Several studies regarding multi-infeed HVDCs and their design procedures have been conducted; however, there are only a few studies explicitly focusing on the MILM system. The study of multi-infeed of LCC and VSC-HVDC may be similar, but it does not fully show the characteristics of MMC-HVDC. Additionally, determining the *PQ* operating region of MMC-HVDC at the converter level does not guarantee its actual performance when integrated into the power system. The requirements of MILM and determination of actually required *PQ* operating region with detailed parameters of MMC-HVDC must be understood for successful integration. If the detailed reactive power consumption is not properly analyzed while designing MMC-HVDC for the MILM system, the MMC-HVDC cannot function properly as the power system requirements, and also, the MILM system may issue related voltage stability. Hence, the MMC-HVDC should be designed based on the actual reactive power requirements, i.e., reactive power consumptions within the MMC-HVDC system for a set of component selections and the feasible grid operating conditions as follows: (1) different values of arm inductance (L_{arm}) and transformer leakage impedance (x_{tr}) determined by manufacturers, (2) variation in system strength or short circuit capacity (SCC), (3) variation in angle spread between MILM terminal and power system, (4) power variation in LCC-HVDC, and (5) maintaining voltage at point of common coupling (PCC) (V_{PCC}) to 1 per unit (pu). This paper suggests a generic analysis framework to determine the exact maximum active/reactive power capability (MPQC) of MMC-HVDC by accurately calculating exact reactive power consumptions within the MILM system through PQ loading analysis. The PQ loading analysis accurately calculates reactive power from MMC-HVDC (Q_{MMC}) to compensate reactive power consumption in MILM system for stable power delivery. The proposed framework determines the required submodule capacitance (C_{sm}) and modulation index (m) of MMC-HVDC by a simple comparison of the MPQC and PQ loading curves.

2. Overview of the Generic Analysis Framework

Figure 1 presents the overall circuit diagram of LCC and MMC-HVDC integrated into MILM system and the MMC structure. The MMC HVDC consists of 6 arms. In each phase, the upper arm is located between the positive DC and AC terminals, and the lower arm is located between the negative DC and AC terminals. The voltage between positive DC terminal and negative DC terminal is V_{DC}. v_u and i_u are the instantaneous upper arm voltage and current, respectively. v_l and i_l are the instantaneous lower arm voltage and current, respectively. Each upper and lower arm has a number of submodule (N_{sm}) with submodule voltage (V_{sm}) and an arm inductor L_{arm} for protection and smoothing. Figure 2 shows a brief flowchart of the generic analysis framework process. The required inputs, such as grid information at the interconnection point, DC voltage and rating of MMC-HVDC (S_{MMC}), and existing LCC-HVDC information, are required to proceed with the generic analysis framework to determine MPQC of MMC-HVDC. MPQC curve formulation is based on the energy calculation of the MMC-HVDC for verifying its rating through selecting values of submodule capacitance and modulation index [35,37].

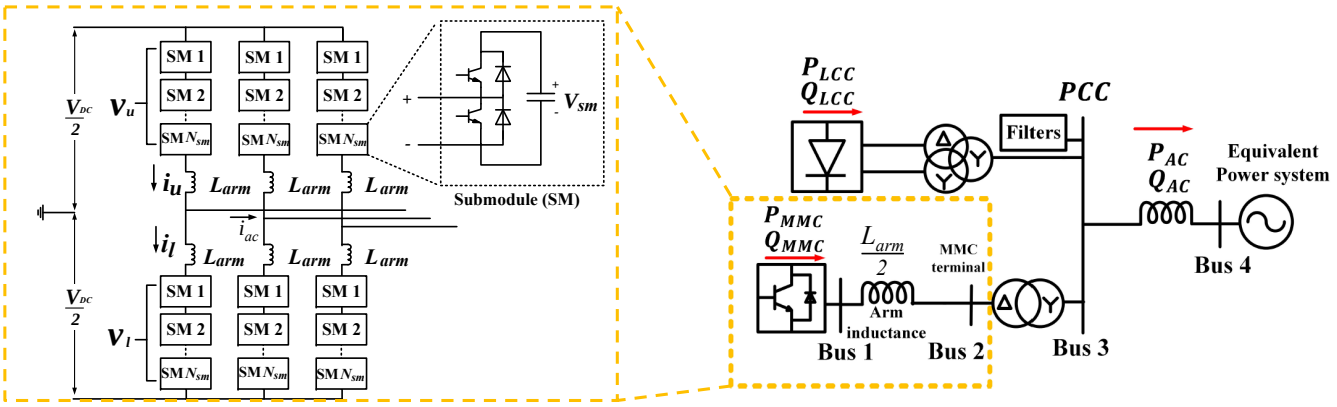

Figure 1. The overall circuit diagram of LCC and MMC-HVDC integrated into MILM system and the MMC structure.

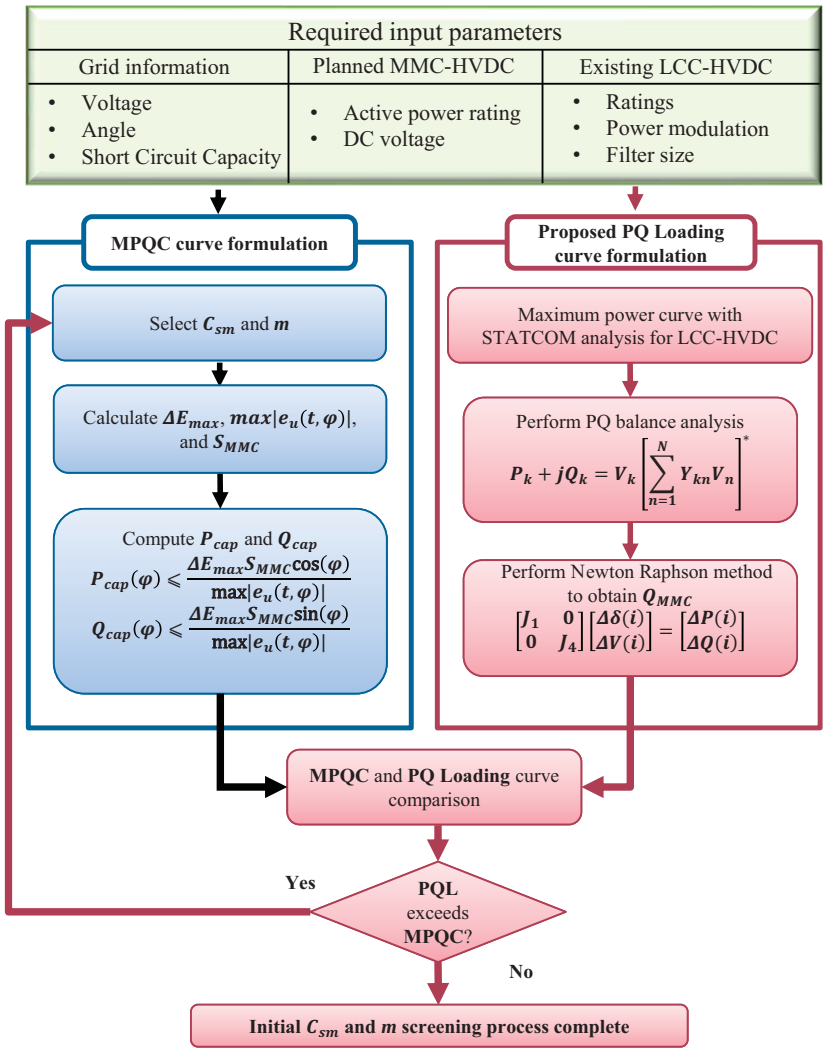

MPQC: Maximum PQ capability

STATCOM: Static Synchronous Compenstator

Figure 2. Generic analysis framework for estimating submodule capacitance and modulation index of MMC-HVDC in MILM.

The importance of reactive power consumptions in the arm reactor (Q_{arm}) and transformer (Q_{tr}) of MMC has never been studied in detail. This paper numerically and visually presents how arm inductance and transformer leakage impedance determined differently by manufacturers can cause a difference in mapping MPQC. This analysis is important because each manufacturer has its own philosophy in designing MMCs that results in different Q_{arm} and Q_{tr}. The change in short circuit capacity of the network directly changes the power flow between PCC and the power system. The power injection to the power system in the MILM system becomes larger than that of a single-infeed system that also changes the power flow. LCC-HVDC induces AC/DC interaction due to its incapability of supporting the grid under different operating points. MMC-HVDC must have Q_{MMC} to balance the power flow and maintain V_{PCC} at 1 pu to balance out the changes in power flow. This implies that a proper MMC-HVDC in MILM should support the reactive powers which are Q_{arm}, Q_{tr}, and reactive power consumption in the system impedance (Q_{sys}) and LCC-HVDC system (Q_{LCC}) to maintain V_{PCC} at 1 pu. This paper proposes the PQ loading analysis resulting in a curve formulation to identify exact Q_{MMC} under given L_{arm}, x_{tr}, and system impedance. Therefore, an equivalent circuit must be developed for power flow analysis between MMC-HVDC and the power system. This process generates the PQ loading curve of MMC-HVDC that considers all the reactive power exchange at PCC. The PQ loading curve varies under different L_{arm}, x_{tr}, system impedance, and the LCC-HVDC system, especially in the MILM case. This paper proposes an enhanced maximum power curve (MPC) analysis, called maximum power curve with static synchronous compensator (STATCOM), to consider AC/DC interaction of LCC-HVDC. This process accurately determines Q_{MMC} when the operating point of LCC-HVDC changes. The maximum power curve with STATCOM can be conveniently embedded into the PQ loading formulation. Finally, the comparison of MPQC and PQ loading curves verified the adequateness of the designed MMC-HVDC. The MMC-HVDC is considered to be adequately designed with sufficient energy to deliver Q_{MMC} to fully support the AC/DC interaction in LCC-HVDC, reactive power consumptions within MMC-HVDC, and power system if the MPQC curve is larger than the PQ loading curve at the point of required active power. The design of MMC-HVDC for maintaining V_{PCC} at 1 pu in MILM can be ultimately achieved through the proposed generic analysis framework.

3. Maximum PQ Capability in MMC-HVDC

There must be a voltage ripple limit in the submodule because the voltage in each submodule continuously changes over time due to the charging and discharging of the capacitor. Therefore, k_{max} is introduced in Reference [35,37]. The excess energy allowed to be stored in one arm, ΔE_{max}, can be written as shown in (1) [35,37].

$$\Delta E_{max} = \frac{N_{sm}}{2} C_{sm} V_{sm.nom}^2 \left(k_{max}^2 - 1,\right) \tag{1}$$

where N_{sm} represents the number of submodule, $V_{sm.nom}$ denotes nominal submodule voltage, and k_{max} represents maximum limit of voltage ripple.

The maximum excess arm energy can also be obtained from the maximum value of the energy variation at a steady state. The energy variation of the upper arm ($e_u(t, \varphi)$), in this case, can be written as shown in (2) by integrating the instantaneous power of the upper arm, which is the product of the arm voltage and current [35].

$$e_u(t, \varphi) = \tfrac{1}{3\omega} S_{MMC} \left(\tfrac{1}{m} \sin(\omega t + \varphi) - \tfrac{1}{2} m \cos(\varphi) \sin(\omega t) - \tfrac{1}{4} \sin(2\omega t + \varphi) \right). \tag{2}$$

As mentioned earlier, the maximum value of the energy variation at a steady-state must be identical to the maximum excess arm energy, as shown in (3).

$$max|e_u(t, \varphi)| = \Delta E_{max}. \tag{3}$$

Based on this information, the equation for determining an overall rating of the MMC, S_{MMC}, can be derived and reorganized as follows:

$$S_{MMC} = \min\left(\frac{\frac{3}{2}\omega N_{sm} C_{sm} V_{sm.nom}^2 \left(k_{max}^2 - 1\right)}{\left|\left(\frac{1}{m} - \frac{m}{2}\right)\sin(\omega t) - \left(\frac{1}{4}\sin(2\omega t)\right)\right|}\right). \tag{4}$$

From (4), it can be concluded that the major components that influence the rating of MMC are N_{sm}, submodule capacitance, $V_{sm.nom}$, k_{max}, and modulation index. The maximum capability range of active power (P_{cap}) and reactive power (Q_{cap}), which imply that MPQC of MMC, can be obtained as follows:

$$P_{cap}(\varphi) \leqslant \frac{\Delta E_{max} S_{MMC} \cos(\varphi)}{\max|e_u(t,\varphi)|}, \tag{5}$$

$$Q_{cap}(\varphi) \leqslant \frac{\Delta E_{max} S_{MMC} \sin(\varphi)}{\max|e_u(t,\varphi)|}. \tag{6}$$

It is possible to produce the MPQC curve of MMC-HVDC based on (5) and (6) indicating the operating range. This paper primarily focuses on the maximum capability of the MMC-HVDC, while the usage of the region within the MPQC is not highlighted.

The MPQC of MMC is mainly influenced by N_{sm}, submodule capacitance, $V_{sm.nom}$, k_{max}, and modulation index. This paper handles the major parameters, such as submodule capacitance, that change the MPQC of the MMC from the design perspective. $V_{sm.nom}$ and N_{sm} are directly related to DC voltage, determined by the rating of cable and IGBT; thus, the change in these two parameters is not analyzed. Consequently, k_{max} is a constraint of MMC design that cannot be varied excessively; therefore, the change in k_{max} is not analyzed.

The parameters given in Table 1 are used to plot the MPQC curve as an example [35]. As shown in Figures 3 and 4, we clearly conclude that the higher value of submodule capacitance and modulation index increases the MPQC of the MMC, when other parameters are fixed. This provides MMC more freedom in positive and negative Q_{cap}, which moves from point A to B.

Figure 4 presents the change in the MPQC curve of the MMC under different settings of modulation index, given that the same values are applied for the rest of the parameters. It is important to note that the value of modulation index in this study implies the maximum value of modulation. It can be concluded that, if the value of modulation index increases, the maximum Q_{cap} increases, where Q_{cap} changes from A to B. The highest possible value of modulation index allows more ancillary service from the MMC, leading to a possible reduction in the size of submodule capacitance for economic perspective.

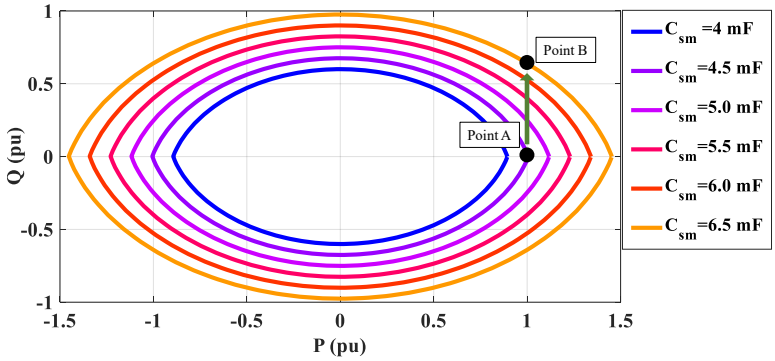

Figure 3. MPQC of MMC under different submodule capacitance values.

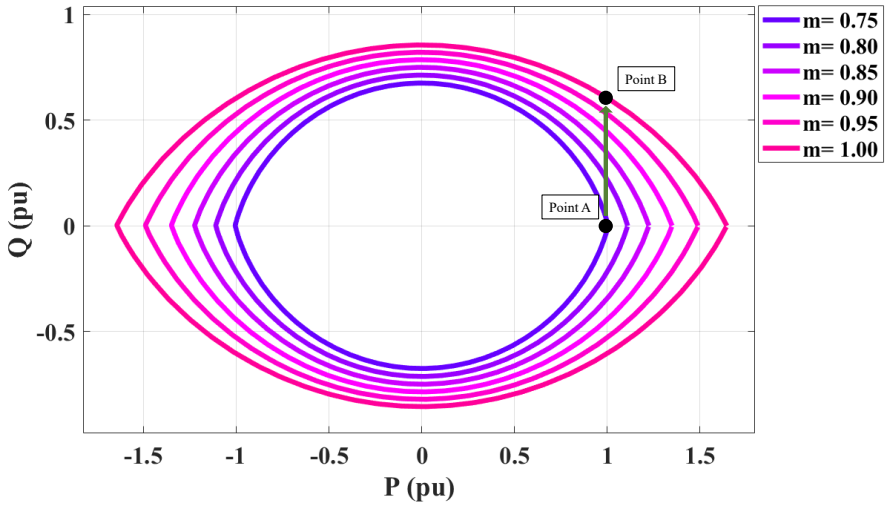

Figure 4. MPQC of MMC under different modulation index values.

Table 1. MMC-HVDC specification for benchmarking Transbay model.

Category	Value	Category	Value
m	0.75	SCC (MVA)	2000
k_{max}	1.1	V_{DC} (kV)	400
S_{MMC} (MVA)	400	$V_{sm.nom}$ (kV)	2
N_{sm}	200	C_{sm} (mF)	4.5

In this section, the value of submodule capacitance and modulation index is one of the key factors in determining the MPQC. The MPQC curve clearly shows the PQ capability of MMC under different factors. However, this analysis alone cannot predict the actual performance. The importance of ancillary service from MMC-HVDC is continuously emphasized in this paper because the MILM system requires strong support from the MMC-HVDC to satisfy five conditions as mentioned before. The next section discusses the procedure to determine the appropriate MPQC of MMC that satisfies the five conditions.

4. PQ Loading Analysis and Curve Formulation

PQ loading analysis is the process of calculating Q_{MMC} that matches reactive power required by the power system for verifying that the value of submodule capacitance and modulation index of MMC form correct MPQC and meets the five conditions. The result of this process can be visualized as a curve, called the PQ loading curve, that can be compared with the MPQC curve to determine if the correct value of submodule capacitance and modulation index is estimated. The basis of PQ loading analysis is power flow calculation by Newton-Raphson method. MMC-HVDC must be converted into a voltage source for power flow analysis [34]. Bus 4 in Figure 1 represents the equivalent power system and the slack bus, where P_4, V_4, and δ_4 are known values. Bus 3 is PCC; it is a PV bus, where the voltage is predetermined to 1 pu, because the objective is to maintain 1 pu. Both V_2 and δ_2 are unknowns in Bus 2. Bus 1 is an artificial bus that does not exist physically; however, it must be defined to correctly calculate Q_{MMC}.

The defined unknown variables are as follows: $u_v = [V_1, V_2]$ and $u_\delta = [\delta_1, \delta_2, \delta_3]$. P_k and Q_k can be formulated as functions of active power and reactive power based on power flow solution, as stated in (7), where x is vector sets of u_v and u_δ. The unknown variables can be solved by the fast decoupled Newton-Raphson method based on the Jacobian matrix, as shown in (8).

$$P_k(\mathrm{x}) = V_k \sum_{n=1}^{N} Y_{kn} V_n \cos(\delta_k - \delta_n - \theta_{kn} + \theta_{tr})$$

$$Q_k(\mathrm{x}) = V_k \sum_{n=1}^{N} Y_{kn} V_n \sin(\delta_k - \delta_n - \theta_{kn} + \theta_{tr}), \tag{7}$$

where $k = 1, 2, \ldots, N$; N implies the number of buses. θ_{tr} implies the 30° shift due to the transformer connecting the MMC-HVDC system.

$$\mathbf{J}_1 = \begin{bmatrix} \partial P_1/\partial \delta_1 & \partial P_1/\partial \delta_2 & \partial P_1/\partial \delta_3 \\ \partial P_2/\partial \delta_1 & \partial P_2/\partial \delta_2 & \partial P_2/\partial \delta_3 \\ \partial P_3/\partial \delta_1 & \partial P_3/\partial \delta_2 & \partial P_3/\partial \delta_3 \end{bmatrix}$$

$$\mathbf{J}_4 = \begin{bmatrix} \partial Q_1/\partial V_1 & \partial Q_1/\partial V_2 \\ \partial Q_2/\partial V_1 & \partial Q_2/\partial V_2 \end{bmatrix}, \tag{8}$$

$$\begin{bmatrix} \mathbf{J}_1 & 0 \\ 0 & \mathbf{J}_4 \end{bmatrix} \begin{bmatrix} \Delta\delta(i) \\ \Delta V(i) \end{bmatrix} = \begin{bmatrix} \Delta P(i) \\ \Delta Q(i) \end{bmatrix}. \tag{9}$$

Finally, all voltage and angle for each bus are calculated based on (9). Q_1, Q_2, Q_3, and Q_4 can be obtained. This process is useful for obtaining Q_{MMC}, as well as for calculating Q consumption in each bus, such as Q_{arm}, Q_{tr}, and Q_{sys}. Thereafter, Q_{MMC} must be iteratively processed from 0 MW to the required P_{MMC} to plot the PQ loading curve.

The blue line in Figure 5 represents the MPQC curve of MMC, designed to only satisfy active power required by the power system without considering reactive power requirement from the power system. For an easier explanation, the right half of the plane of the graphs is an inverter side of MMC. The black line represents the PQ loading curve of the MMC-HVDC, which indicates the required Q_{MMC} in order to maintain V_{PCC} at 1 pu, along with the change in P_{MMC}. If the power system requires P_{MMC} of 1 pu, then Q_{MMC} of 0.22 pu, point B in Figure 6 is required in this case. However, the MMC-HVDC with the blue MPQC curve cannot support reactive power PQ loading curve that exceeds the MPQC curve at P_{MMC}, which indicates point A in Figure 6. If an appropriate increase of submodule capacitance and modulation index is determined, the PQ loading curve stays within the MPQC curve (red and yellow curve) at the desired point. This is the main reason why the correct estimation of Q_{MMC} is important in determining submodule capacitance and modulation index.

There can be various combinations of setting up values between those two parameters. However, modern MMC-HVDC is designed with the highest possible value of modulation index, which is close to 1. Therefore, it is necessary to consider various power system variants when selecting submodule capacitance for the appropriate MPQC of MMC-HVDC in the planning stage.

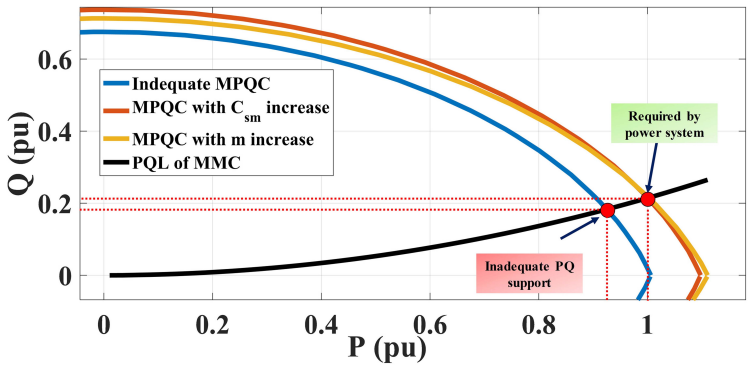

Figure 5. An adequate MMC design for satisfying grid requirement by increasing capacitance to 4.91 mH or modulation index to 0.8.

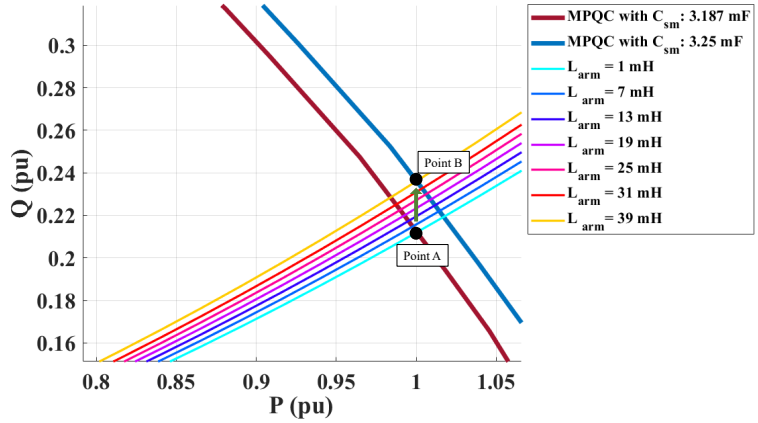

Figure 6. Changes in PQ loading curves of MMC with different arm inductance values.

Manufacturers have their unique ways to determine the value because L_{arm} is determined mainly by the internal stability of the MMC, such as suppressing the circulating current and fault current [44–47]. Consequently, Q_{MMC} varies due to the different Q_{arm} values, which requires different values of submodule capacitance that lead to different MPQC. As shown in Figure 6, the slope of PQ loading curve increases with the increasing L_{arm} value (moving from A to B) under the same parameters of MMC given in Table 1, except the modulation index of 1. This is due to the Q_{arm} ranging from 1% to 20% of the total Q consumption in this case that requires MMC to have higher submodule capacitance to maintain V_{PCC} at 1 pu. Therefore, it is important to determine the value of L_{arm} based on its primary purposes. However, it is worth noting that larger L_{arm} leads to larger submodule capacitance.

A similar context applies to x_{tr} also. The increase in x_{tr} lead to a higher Q_{tr} ranging from 35% to 48% of total reactive power consumption owing to x_{tr} ranging between 0.1 and 0.2 pu. This requires MMC to have higher submodule capacitance, moving from point A to B, to maintain V_{PCC} at 1 pu, as shown in Figure 7. The slope change in the PQ loading curve is bigger than in the previous case because Q_{tr} takes a larger portion than Q_{arm} from the power system perspective.

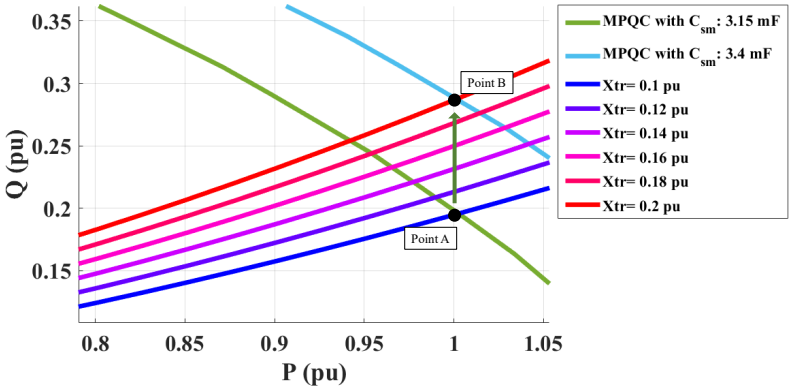

Figure 7. Change in PQ loading curves of MMC with different transformer leakage impedance values.

Finally, the PQ loading curve is mostly influenced by the impedance of the power system, referring to the short circuit capacity or short circuit ratio (SCR). As shown in Figure 8, as the value of short circuit ratio increases, which refers to an increase in system strength, Q_{sys}, which can be as low as 28% of total reactive power consumption, significantly decreases (moving from point B to A). The lower short circuit ratio requires a significant amount of Q_{sys}, which can be as high as 80% of the total reactive power consumption, to maintain V_{PCC} at 1 pu. Therefore, the change in the system strength must be correctly predicted to estimate the correct Q_{MMC} and MPQC.

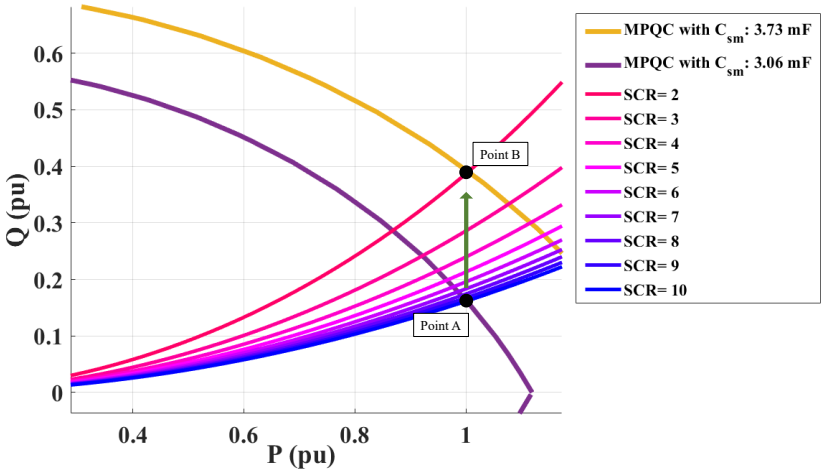

Figure 8. Change in PQ loading curves of MMC with different short circuit ratio values.

This section presents the PQ loading analysis of single-infeed MMC-HVDC integration to power systems under different values of L_{arm}, x_{tr}, and short circuit ratio. The PQ loading curves are portrayed differently due to the nature of the reactive power consumption from each segment. If the values of L_{arm} and x_{tr} are high and the value of short circuit ratio is low, it is inevitable that the cost of MMC-HVDC becomes much higher due to the high demand of Q_{MMC} and MPQC. Therefore, a careful selection of submodule capacitance and modulation index is needed by considering given L_{arm}, x_{tr}, and short circuit capacity to successfully integrate MMC-HVDC not only from the electronic point of view [48] but also from the power system point of view. This consideration becomes more complicated when the MMC-HVDC is integrated close to the existing LCC-HVDC to form MILM because LCC-HVDC is widely known for strong AC/DC interaction.

5. MPQC and PQ Loading in MILM

5.1. Maximum Power Curve with STATCOM Analysis for PQ Loading Analysis in MILM

There have been many studies regarding multi-infeed of LCC-HVDC and VSC-HVDC. However, there are few studies regarding the MILM case, especially to provide a guideline for selecting the correct MPQC of MMC-HVDC from the power system perspective. A general configuration of MILM for the inverter side is portrayed as an example in Figure 1. An analysis of LCC-HVDC must be considered to understand the operating range of MILM from the power system perspective. The operating range of LCC-HVDC without MMC-HVDC in Figure 1 is normally analyzed by MPC [22,24,49]. This provides the operating range of LCC-HVDC and the behavior of AC and DC voltages under different DC currents. It is widely known that a higher short circuit ratio implies more robustness in the voltage deviation on both AC and DC sides.

MPC is a renowned assessment process. There have been studies on steady state operation of HVDC [24,25,30,38,49–53]. MPC portraits a unique relationship between P_{DC}/I_{DC} characteristics, which is directly influenced by short circuit ratio. Equation (10) and Figure 9 present the possible parameters that must be considered in the AC/DC interaction of LCC-HVDC. V_{DC} and i_{DC} refer to the DC voltage and current, respectively. T denotes the transformer winding, B represents the number of a bridge, and x_c denotes the impedance of the transformer.

$$\mathbf{X}_{HVDC} = [E_{ac}, V_{ac}, P_{DC}, V_{DC}, Q_{LCC}, \delta_1, \delta_2, Q_{ac}, I_{comp}, B, T, Z_{inv}, \gamma, x_c, Z_{trans}]^T. \quad (10)$$

Each parameter indicates sending side AC voltage, terminal AC voltage, DC power, DC voltage, reactive power consumption of HVDC converter, sending AC side angle, receiving AC side angle, reactive power from AC side, compensator current, pulse bridge number, transformer ratio, impedance on inverter side, gamma angle, transformer leakage impedance, and transformer leakage in pu, respectively.

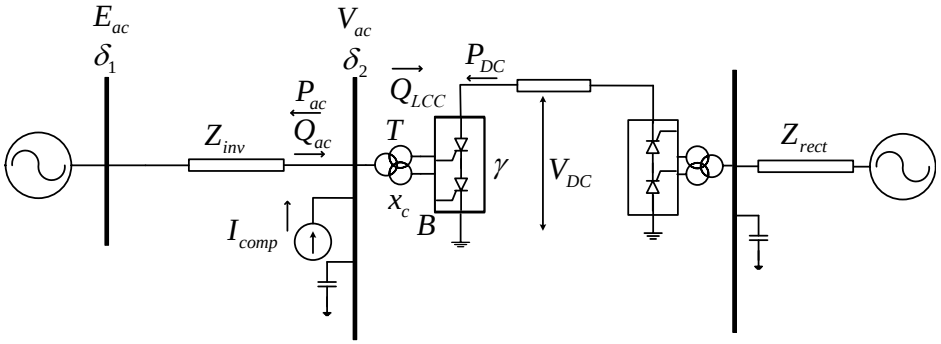

Figure 9. Equivalent AC/DC connection and its parameters for analysis.

Although the derivation of the specific relationship between AC and DC sides has already been done [24,25,30,38,49–53], these equations shown below are based on the concept of PQ exchange between the power and LCC-HVDC systems. This refers to $P_{DC} = P_{ac}$ that emphasize the AC/DC interaction in a more concise manner as a combination of theoretical HVDC and power flow equations for the numerical computation. MPC graphs can be readily obtained by numerically solving the nonlinear equations stated in (11)–(21).

Active power related equations are as follows:

$$P_{DC} - \frac{E_{ac}V_{ac}}{Z_{inv}}\sin(\delta_1 - \delta_2) = 0, \tag{11}$$

$$P_{DC} - V_{DC} \cdot i_{DC} = 0, \tag{12}$$

$$V_{DC} - \frac{3\sqrt{2}}{\pi}V_{ac} \cdot B \cdot T \cdot \cos(\gamma) + \frac{3}{\pi} \cdot x_c \cdot B \cdot i_{DC} = 0, \tag{13}$$

$$P_{DC} - \frac{3\sqrt{2}}{\pi}V_{ac} \cdot B \cdot T \cdot i_{DC} \cdot \cos(\gamma) + \frac{3}{\pi} \cdot x_c \cdot B \cdot i_{DC}^2 = 0. \tag{14}$$

Reactive power related equations:

$$Q_{ac} + \frac{V_{ac}^2}{Z_{cap}} - Q_{LCC} = 0, \tag{15}$$

$$Q_{ac} - \frac{E_{ac}V_{ac}}{Z_{inv}}\cos(\delta_1 - \delta_2) + \frac{V_{ac}^2}{Z_{ac}} = 0, \tag{16}$$

$$Q_{LCC} - P_{DC} \cdot \tan(\theta) = 0, \tag{17}$$

$$Q_{LCC} - P_{DC} \cdot \tan\theta - \tan(\cos^{-1}(\frac{V_{DC}}{V_{DC} + \frac{3}{\pi}x_c \cdot B \cdot i_{DC}})) = 0, \tag{18}$$

$$Q_{LCC} - \frac{E_{ac}V_{ac}}{Z_{inv}}\cos(\delta_1 - \delta_2) + \frac{V_{ac}^2}{Z_{inv}} - \frac{V_{ac}^2}{Z_{cap}} = 0, \tag{19}$$

$$\tan\theta - \tan(\cos^{-1}(\frac{V_{DC}}{V_{DC} + \frac{3}{\pi}x_c \cdot B \cdot i_{DC}})) = 0, \tag{20}$$

$$x_c = \frac{(V_{ac} \cdot T)^2}{P_{DC}}Z_{trans}. \tag{21}$$

Once all the computations are finished, it is possible to obtain the MPC curve of the LCC-HVDC system that portraits profiles of DC power, terminal voltage, DC voltage, and reactive power consumption from the converter of HVDC in different system strengths. The conventional MPC analysis shows the AC/DC interaction of the LCC-HVDC system such that voltage deviation as the operating point of LCC-HVDC varies. The voltage deviation caused by the LCC-HVDC system violates the last three of the five conditions in

MILM system. This can trigger MMC-HVDC to exceed its operation limit or to operate it with unsatisfying performance. The voltage supporters, such as STATCOM, must be applied to prevent the AC/DC interaction. MMC-HVDC can operate as STATCOM in the case of MILM.

Therefore, maximum power curve with STATCOM is introduced that numerically explained the steady-state analysis of LCC-HVDC and STATCOM and prevents LCC-HVDC from AC/DC interaction by determining exact Q_{MMC}. Besides the nonlinear equations stated above, Equation (22) is added to the numerical solving process. This allows the observation of the steady V_{DC} and V_{ac} of the LCC-HVDC system when the reactive current (i_{comp}) reaches its maximum rating ($i_{comp.max}$). As shown in Figure 10, the power transfer capability of LCC-HVDC is stabilized with the support of STATCOM due to the steady terminal AC voltage in every DC current operation, which is different from conventional MPC results. Theoretically, an ideal compensator allows the DC power to have nearly a linear relationship with the DC current under any AC system strength. A practical STATCOM compensates reactive power up to its maximum value to maintain the terminal voltage constantly. However, the voltage starts to deviate when the reactive power from STATCOM, Q_{comp}, exceeds its maximum capability. Based on maximum power curve with STATCOM analysis, the voltage deviation due to the operation of LCC-HVDC from 0 to 1 pu can be well predicted, as well as how much of Q_{MMC} must be supplied from MMC-HVDC to maintain V_{PCC} of 1 pu in the MILM system.

$$Q_{LCC} = \frac{E_{ac}V_{ac}}{Z_{ac}}\cos(\delta_1 - \delta_2) + \frac{V_{ac}^2}{Z_{ac}} - \frac{V_{ac}^2}{Z_{cap}} + V_{ac}i_{comp}, \tag{22}$$

where $|i_{comp}| \leqslant |i_{comp.\max}|$.

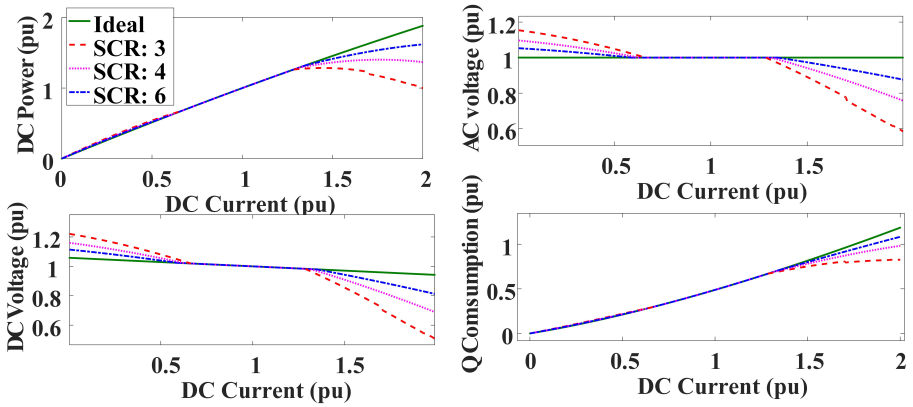

Figure 10. Maximum power curve with STATCOM result from LCC-HVDC perspective.

The PQ loading curve formulation for MILM is similar to (7) and (8), except for the reactive power exchange in PCC analysis based on maximum power curve with STATCOM result. In this case, it is possible to identify LCC-HVDC system as the negative variable PQ load with the following equations:

$$P_{LCC} = (((3\sqrt{2}/\pi)V_{PCC}TB\cos(\gamma)) - ((3/\pi)x_cBi_{DC})))i_{DC}, \tag{23}$$

$$Q_{LCC} = P_{LCC}\tan(\cos^{-1}(V_{DC}/(V_{DC} + (3/\pi)Bx_ci_{DC}))), \tag{24}$$

$$(Q_{MMC} - Q_{arm} - Q_{tr}) + Q_{filter} - Q_{LCC} - Q_{ac} = 0. \tag{25}$$

Equations (23) and (24) add the operating characteristic of LCC-HVDC to PCC, which bring AC/DC interaction. Equation (25) provides all the reactive power exchanges at PC,C including reactive power consumptions in MMC and LCC-HVDC, and system impedance.

With this additional condition, unknown variables mentioned previously can be solved, and it is possible to obtain updated Q_{MMC}.

5.2. Estimation of Correct MPQC Based on PQ Loading Analysis in MILM

Like the MPQC analysis of the single MMC, the determination of correct MPQC based on PQ loading analysis considering all five conditions must be processed in MILM. The PQ loading curves in Figure 11 clearly show that the slope of the PQ loading curve for MILM is much steeper, even though MMC-HVDC delivers the same power, in both cases. This is the case where both HVDCs have the same power rating delivering active power in the same direction.

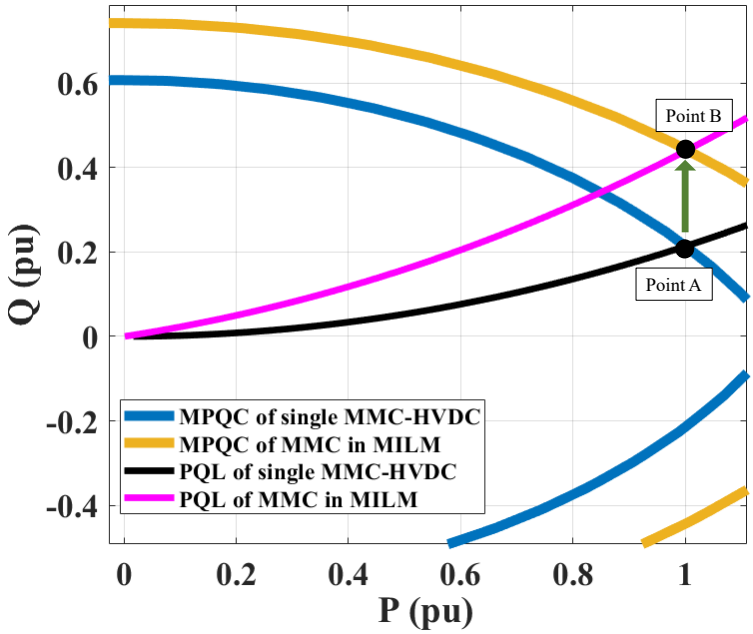

Figure 11. Steeper PQ loading curve in MILM causing higher requirement of MPQC.

This causes the Q_{MMC} to move from point A to B. The angle spread between the phase of the PCC, δ_{PCC}, and the system, δ_s, becomes larger, and the reactive power requirement from the power system changes based on the power flow analysis, while the P delivered into receiving end increases.

Figures 11–14 present several different cases to prepare the MMC-HVDC specification under the MILM. Various short circuit ratio, operations in LCC-HVDC, and system voltages should be considered for the correct MPQC determination of MMC-HVDC in MILM system. Figures 11 and 12 have a similar pattern to that in Figure 8, where the low short circuit ratio requires higher Q_{MMC} (moving from point A to B). However, receiving end receives more power, and short circuit ratio lowers due to (26), where the value of $P_{MMC,max}$ and $P_{LCC,max}$ is rated power. This causes PQ loading curves to become steeper than those in Figure 8, even though the short circuit capacity value is the same. Therefore, MMC-HVDC can support the MILM system under short circuit capacity variation on the interconnecting point to satisfy the five conditions.

$$SCR = \frac{SCC}{P_{MMC,max} + P_{LCC,max}}. \tag{26}$$

As shown in Figure 13, the MMC-HVDC must operate in a diverse range under different LCC-HVDC operating points. It is worth noting that this analysis does not include the sequence of filters attached to the LCC-HVDC system because the operating strategy is not included at this stage. When P_{MMC} is zero, MMC-HVDC is operated as STATCOM to absorb reactive power when LCC-HVDC is operating under 1 pu and deliver reactive power when it is operating over 1 pu of active power, which means temporary

overloading condition. Point A is considered the proper design point when both LCC and MMC-HVDC operated within 1 pu of active power. If the existing LCC-HVDC performs with overloading state and MMC-HVDC operates at 1 pu for delivering extra power to the system, the design point moves to B. However, if LCC-HVDC chooses to overload and MMC-HVDC operates under the previous MPQC, which is point C, the total power delivered to the system is identical to point A. Therefore, it must be determined whether the MMC-HVDC should have MPQC that embraces the overloading operation of the LCC-HVDC system based on the need of the system.

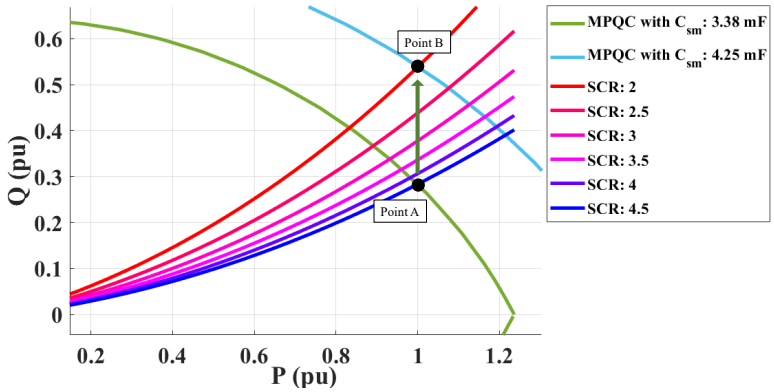

Figure 12. Different PQ loading curves of MMC in MILM under different short circuit ratio.

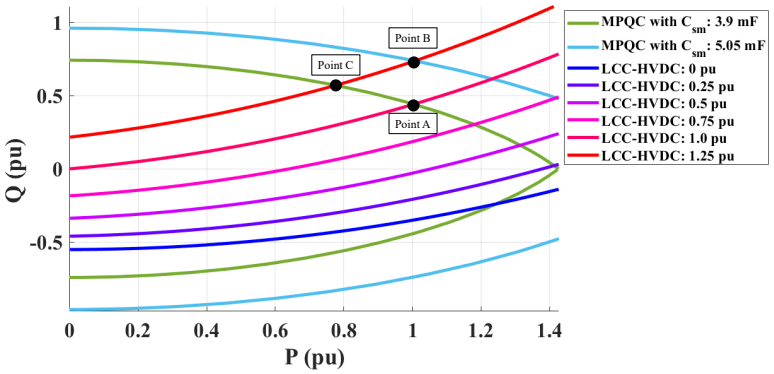

Figure 13. Different PQ loading curves of MMC in MILM case under different LCC-HVDC operating points.

Finally, the deviation in the system voltage must be considered in designing MMC-HVDC. If the system voltage deviates due to a disturbance, the decreased system voltage requires a higher Q_{MMC} (moving from point A to B) to stabilize both the power system and LCC-HVDC, as shown in Figure 14. When the system voltage exceeds 1 pu, MMC-HVDC absorbs reactive power to maintain V_{PCC} at 1 pu. However, absorbing reactive power does not significantly affect the determination of submodule capacitance because the MMC-HVDC has more reactive power absorbing capability, as shown in Figure 14.

Therefore, the analyses imply that the power system with low short circuit ratio, LCC-HVDC operating with rated power or higher, and low system voltage requires a tremendous amount of Q_{MMC} to deliver the required active and reactive power that maintain a stable power system. The parameters must be carefully determined for MMC-HVDC to operate properly and to support power system effectively under the given condition.

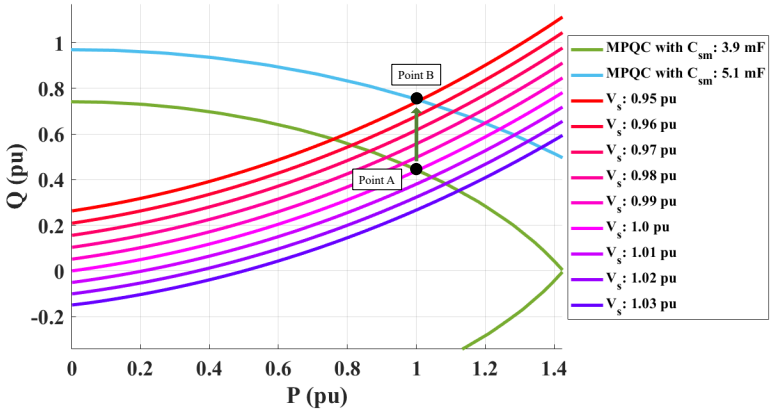

Figure 14. Different PQ loading curves of MMC in MILM case under different system voltages.

5.3. Application of the Proposed Method for MMC-HVDC of Jeju MILM System

The project to connect the mainland of South Korea and Jeju Island with MMC-HVDC is an important issue in South Korea. Jeju Island is located in the southern part of South Korea, and its power system is totally islanded, as shown in Figure 15. Jeju Island has been designated as a zero carbon project with large-scale wind power implementation because of the availability of wind energy sources. Its peak load was approximately 912 MW in 2017 [54]. This massive wind power penetration surpasses the peak load of Jeju Island and requires power transmission back to the mainland power system. There are two LCC-HVDCs (300 and 400 MW) that deliver power to Jeju from the mainland. Approximately 273 MW of the wind farm is in operation; Korea Electric Power Corporation (KEPCO), the nation's only utility, has proposed that the capacity of the wind farm will reach 2 GW by 2030 [55,56]. The rest of the power will be sent back to the mainland through the HVDCs because the power generated in Jeju is expected to surpass the load demand. The topology of Jeju HVDC No. 3 (200 MW, under construction [54]) is VSC-HVDC because VSC-HVDC enables fast power control and continuous power reversal. The feasibility study of MMC-HVDC, Jeju HVDC No. 3, is currently underway to support the existing Jeju HVDC No. 1 and the power flow control of the expected high wind farm, as shown in Figure 15. However, the government-led project, called "Carbon Zero Island", and the increasing load in Jeju has initiated an increase in wind power penetration in Jeju. A total of 2000 MW of wind power facilities will be introduced by 2030, which will cause a dramatic reduction in short circuit capacity from 3000 to 1000 MVA due to the shut down of conventional generators. Therefore, the correct MPQC estimation of the MMC-HVDC in Jeju HVDC No. 3 is necessary to efficiently cooperate with neighboring HVDCs.

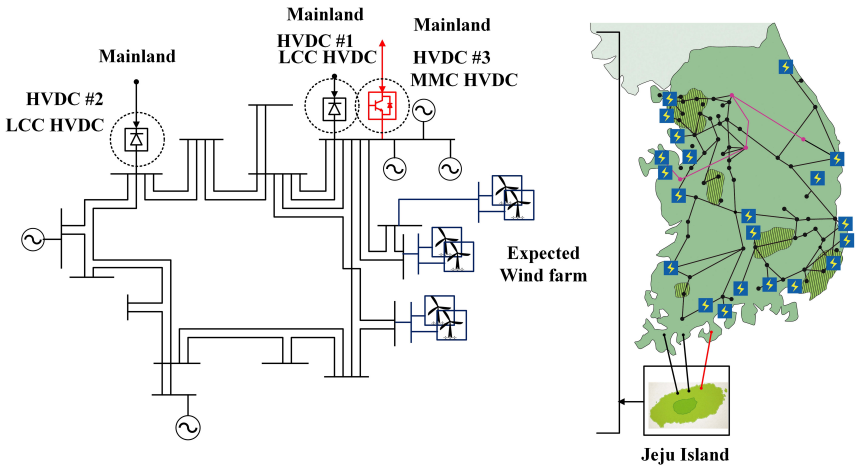

Figure 15. Simple representation of Jeju Island power system for possible MILM scenario in the future.

Table 2 and Figure 16 show the expected PQ loading and MPQC curves for Jeju HVDC No. 3. Q_{MMC} must be at least 147 Mvar to maintain a constant V_{PCC}, LCC-HVDC operation, and support the power system (point A) due to the lowered short circuit capacity. Consequently, pre-installed filters of Jeju HVDC No. 1 deviates V_{PCC} causing Jeju HVDC No. 3 to operate STATCOM mode if P_{MMC} is zero. While Jeju HVDC No. 3 must transfer the active power back to the mainland due to excessive wind power in the future, planning for the MPQC of the rectifier mode is also necessary. The requirement of Q_{MMC} in rectifier mode is lower than that of in inverter mode (point B) due to the pre-installed filters. Therefore, only the inverter mode is critical in determining the parameters of Jeju HVDC No. 3.

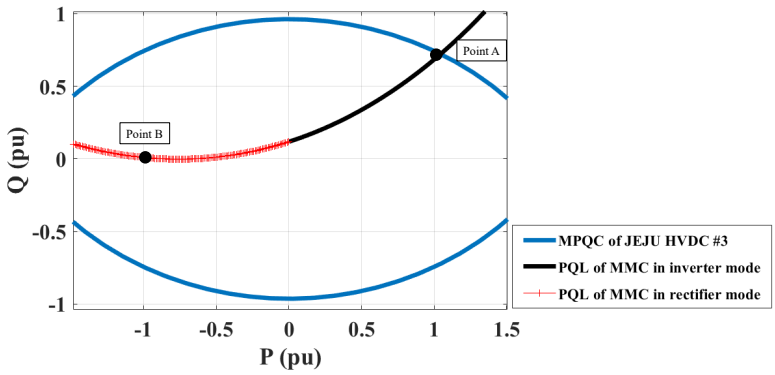

Figure 16. The PQ loading curve required from MMC-HVDC in Jeju Island considering bidirectional power flow in MILM case under lowered short circuit capacity due to the high penetration of wind power.

A detailed PSCAD simulation was performed by modeling the Jeju MILM case to prove the numerical analysis. While 500 MW is delivered to the power system with short circuit capacity of 1000 MVA, MMC-HVDC with the estimated submodule capacitance and low submodule capacitance are compared. Finally, the MMC-HVDC with the estimated submodule capacitance operates within 10% of voltage ripples in the capacitor, as shown in Figure 17. Therefore, the numerical procedure for designing MMC-HVDC in MILM can be verified.

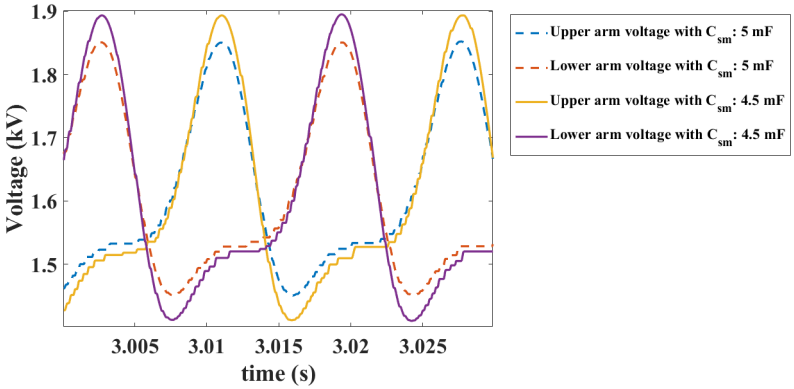

Figure 17. Validation of numerical analysis using PSCAD through observing voltage ripple of the submodule in MMC-HVDC in Jeju MILM case.

The generic analysis framework is not limited to the single scenario in the MILM system. The parameter shown in Table 2 are only for performing appropriately under given short circuit capacity, arm reactor, transformer leakage impedance, LCC-HVDC operation, and system voltage. This fixed operating point may not perform as desired under the change in the system. The generic analysis framework can be applied to find an operating range for MMC-HVDC that covers the variable conditions. PQ loading curve

for the maximum reactive power absorption and generation cases can be determined. If MMC-HVDC is required to perform under changing short circuit capacity, LCC-HVDC operation, and system voltage and if the value of arm reactor and transformer leakage impedance is not completely determined.

Table 2. Parameter estimation for Jeju HVDC No. 3.

Category	Value	Category	Value
m	0.9	SCC (MVA)	1000
$P_{LCC,max}$ (MW)	300	V_{DC} (kV)	300
$P_{MMC,max}$ (MW)	200	$V_{sm.nom}$ (kV)	1.65
V_{PCC} (kV)	154	C_{sm} (mF)	5
V_t (kV)	165	Q_{MMC} (MVAR)	147

There can be five variable conditions, as shown in Table 3. There can be 30 cases to be tested within the ranges of the variable conditions to verify if the initial estimation of the HVDC parameter can handle these conditions. Among the cases, there are cases where PQ loading curves exceed MPQC curves with 5 mF, implying that the energy of the MMC is not enough to support LCC-HVDC, the power system, and itself. The maximum reactive power absorption and generation case must be identified to satisfy all the conditions, as shown in Table 4. Approximately 7 mF of capacitor value is required; the operation range is shown in Figure 18. This proposed generic analysis framework can determine minimum energy required by MMC considering various system conditions. It is worth noting that the values of L_{arm} and x_{tr} are not changing variables from the MMC-HVDC operation perspective. The values must be fixed within the given range during planning studies for their specific purposes, and then the values can be applied to calculate the appropriate PQ loading curve for obtaining an accurate Q_{MMC} under different operating scenarios.

Table 3. Possible combinations of parameters for Jeju HVDC No. 3 to determine the full operating region.

Category	Value
SCC (MVA)	1000–3000
L_{arm} (mH)	1–100
x_{tr} (pu)	0.1–0.2
P_{LCC} (pu)	0–1
System voltage (pu)	0.95–1.05
$P_{LCC,max}$ (MW)	300
$P_{MMC,max}$ (MW)	200
m	0.925
V_{DC} (kV)	300

Table 4. Maximum reactive power absorption and generation case for Jeju HVDC No. 3.

Category	Maximum Q Absorption Case	Maximum Q Generation Case
SCC (MVA)	3000	1000
L_{arm} (mH)	1	100
x_{tr} (pu)	0.1	0.2
P_{LCC} (pu)	0	1
System voltage (pu)	1.05	0.95

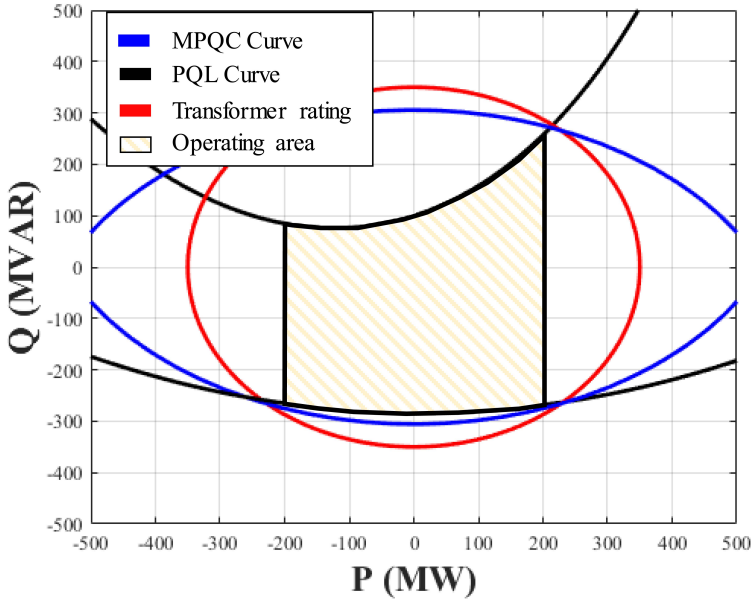

Figure 18. Representation of MMC operation range satisfying all conditions with submodule capacitance of 7 mF.

6. Conclusions

This paper proposes a generic analysis framework that can develop a grid supporting MMC-HVDC in the MILM system. It was initiated to support the utility and manufacturer for the Jeju HVDC No. 3 project in South Korea. The comparison of MPQC and PQ loading curve conveniently indicates the proper value of submodule capacitance and modulation index of MMC-HVDC system, allowing MMC-HVDC to support sufficient reactive power to the MILM system to compensate for reactive power consumptions. Reactive power consumption within the MMC-HVDC systems, such as arm reactor and transformer leakage impedance, and reactive power consumption in LCC-HVDC system, and reactive power consumption in the power system is comprehensively calculated through PQ loading analysis. The theoretical result is verified by the PSCAD/EMTDC simulation that MMC-HVDC operates within the maximum voltage ripple limit through utilizing the calculated value of submodule capacitance. The proposed method is applied to the MILM system in Jeju island. The largest Q_{MMC} absorption and generation cases are determined by defining five variable conditions. Finally, the required operating range for MMC-HVDC is determined, resulting in the proper values of submodule capacitance and modulation index of the MMC-HVDC system. The generic analysis framework is not limited to the single scenario in the MILM system. It can be applied to find the desired operating range for MMC-HVDC and MPQC that covers the variable conditions when the MMC-HVDC is required to perform under changing short circuit capacity, LCC-HVDC operation, system voltage, and various values of L_{arm} and x_{tr}. Therefore, the framework can help grid planners and manufacturers to develop MMC-HVDC that performs under various power system conditions. Ultimately, the proposed framework provides the initial values to the detailed EMTDC study without an iterative time-consuming modeling process of MMC-HVDC.

Author Contributions: Conceptualization, S.K., K.H. and H.K.; methodology, S.K. and H.K.; software, S.K. and H.K.; validation, S.K., K.H., J.N. and H.K.; formal analysis, S.K. and H.K.; investigation, S.K.; resources, J.Y.; data curation, S.K.; writing—original draft preparation, S.K.; writing—review and editing, K.H., J.N. and H.K.; visualization, J.N.; supervision, H.K.; project administration, K.H.; funding acquisition, K.H. and J.Y. All authors have read and agreed to the published version of the manuscript.

Funding: This research was supported by Korea Electric Power Corporation.(Grant number: R17TG04). This work was supported under the framework of international cooperation program managed by National Research Foundation of Korea (Grant number: 2017K1A4A3013579).

Institutional Review Board Statement: Not applicable.

Informed Consent Statement: Not applicable.

Data Availability Statement: Not applicable.

Conflicts of Interest: The authors declare no conflict of interest.

References

1. Jovicic, D.; Ahmed, K. *High Voltage Direct Current Transmission: Converters, Systems and DC Grids*, 1st ed.; Wiley: Chichester, UK, 2015.
2. Report, I.C. Dynamic Performance Characteristics of North American HVDC Systems for Transient and Dynamic Stability Evaluations. *IEEE Trans. Power Appar. Syst.* **1981**, *PAS-100*, 3356–3364. [CrossRef]
3. Taylor, C.W.; Lefebvre, S. HVDC controls for system dynamic performance. *IEEE Trans. Power Syst.* **1991** , *6*, 743–752. [CrossRef]
4. Lee, R.L.; Beshir, M.J.; Gee, J.H. Planning Considerations for the Intermountain HVDC Transmission System. *IEEE Trans. Power Del.* **1986**, *1*, 225–231. [CrossRef]
5. Lee, R.L.; Melvold, D.J.; Szumlas, D.J.; Le, L.M.; Finley, A.T.; Martin, D.E.; Wong, W.K.; Dickmander, D.L. Potential DC system support to enhance AC system performance in the Western United States. *IEEE Trans. Power Syst.* **1993**, *8*, 264–274. [CrossRef]
6. Flourentzou, N.; Agelidis, V.G.; Demetriades, G.D. VSC-Based HVDC Power Transmission Systems: An Overview. *IEEE Trans. Power Electron.* **2009**, *24*, 592–602. [CrossRef]
7. Nami, A.; Liang, J.; Dijkhuizen, F.; Demetriades, G.D. Modular Multilevel Converters for HVDC Applications: Review on Converter Cells and Functionalities. *IEEE Trans. Power Electron.* **2015**, *30*, 18–36. [CrossRef]
8. Debnath, S.; Qin, J.; Bahrani, B.; Saeedifard, M.; Barbosa, P. Operation, Control, and Applications of the Modular Multilevel Converter: A Review. *IEEE Trans. Power Electron.* **2015**, *30*, 37–53. [CrossRef]
9. Qin, J.; Saeedifard, M. Predictive Control of a Modular Multilevel Converter for a Back-to-Back HVDC System. *IEEE Trans. Power Del.* **2012**, *27*, 1538–1547. [CrossRef]
10. Du, C.; Bollen, M.H.J.; Agneholm, E.; Sannino, A. A New Control Strategy of a VSC HVDC System for High-Quality Supply of Industrial Plants. *IEEE Trans. Power Del.* **2007**, *22*, 2386–2394. [CrossRef]
11. Perez, M.A.; Rodriguez, J.; Fuentes, E.J.; Kammerer, F. Predictive Control of AC-AC Modular Multilevel Converters. *IEEE Trans. Ind. Electron.* **2012**, *59*, 2832–2839. [CrossRef]
12. Son, G.T.; Lee, H.J.; Nam, T.S.; Chung, Y.H.; Lee, U.H.; Baek, S.T.; Hur, K.; Park, J.W. Design and Control of a Modular Multilevel HVDC Converter With Redundant Power Modules for Noninterruptible Energy Transfer. *IEEE Trans. Power Del.* **2012**, *27*, 1611–1619. [CrossRef]
13. Gnanarathna, U.N.; Gole, A.M.; Jayasinghe, R.P. Efficient Modeling of Modular Multilevel HVDC Converters (MMC) on Electromagnetic Transient Simulation Programs. *IEEE Trans. Power Del.* **2011**, *26*, 316–324. [CrossRef]
14. Saad, H.; Dennetière, S.; Mahseredjian, J.; Delarue, P.; Guillaud, X.; Peralta, J.; Nguefeu, S. Modular Multilevel Converter Models for Electromagnetic Transients. *IEEE Trans. Power Del.* **2014**, *29*, 1481–1489. [CrossRef]
15. Saeedifard, M.; Iravani, R. Dynamic Performance of a Modular Multilevel Back-to-Back HVDC System. *IEEE Trans. Power Del.* **2010**, *25*, 2903–2912. [CrossRef]
16. Moon, J.W.; Kim, C.S.; Park, J.W.; Kang, D.W.; Kim, J.M. Circulating Current Control in MMC Under the Unbalanced Voltage. *IEEE Trans. Power Del.* **2013**, *28*, 1952–1959. [CrossRef]
17. Tu, Q.; Xu, Z.; Chang, Y.; Guan, L. Suppressing DC Voltage Ripples of MMC-HVDC Under Unbalanced Grid Conditions. *IEEE Trans. Power Del.* **2012**, *27*, 1332–1338. [CrossRef]
18. Liu, G.; Xu, Z.; Xue, Y.; Tang, G. Optimized Control Strategy Based on Dynamic Redundancy for the Modular Multilevel Converter. *IEEE Trans. Power Electron.* **2015**, *30*, 339–348. [CrossRef]
19. Jung, J.J.; Lee, J.H.; Sul, S.K.; Son, G.T.; Chung, Y.H. DC Capacitor Voltage Balancing Control for Delta-Connected Cascaded H-Bridge STATCOM Considering Unbalanced Grid and Load Conditions. *IEEE Trans. Power Electron.* **2018**, *33*, 4726–4735. [CrossRef]
20. Jung, J.J.; Cui, S.; Lee, J.H.; Sul, S.K. A New Topology of Multilevel VSC Converter for a Hybrid HVDC Transmission System. *IEEE Trans. Power Electron.* **2017**, *32*, 4199–4209. [CrossRef]
21. Lee, J.H.; Jung, J.J.; Sul, S.K. Balancing of Submodule Capacitor Voltage of Hybrid Modular Multilevel Converter Under DC-Bus Voltage Variation of HVDC System. *IEEE Trans. Power Electron.* **2019**, *34*, 10458–10470. [CrossRef]
22. Gavrilovic, A. AC/DC system strength as indicated by short circuit ratios. In Proceedings of the International Conference on AC and DC Power Transmission, London, UK, 17–20 September 1991; pp. 27–32.
23. Jovcic, D.; Pahalawaththa, N.; Zavahir, M. Small signal analysis of HVDC-HVAC interactions. *IEEE Trans. Power Del.* **1999**, *14*, 525–530. [CrossRef]
24. Reeve, J.; Uzunovic, E. Study of power transfer capability of DC systems incorporating AC loads and a parallel AC line. *IEEE Trans. Power Del.* **1997**, *12*, 426–434. [CrossRef]

25. Aik, D.L.H.; Andersson, G. Voltage stability analysis of multi-infeed HVDC systems. *IEEE Trans. Power Del.* **1997**, *12*, 1309–1318. [CrossRef]
26. Karawita, C.; Annakkage, U.D. Multi-Infeed HVDC Interaction Studies Using Small-Signal Stability Assessment. *IEEE Trans. Power Del.* **2009**, *24*, 910–918. [CrossRef]
27. Rahimi, E.; Gole, A.M.; Davies, J.B.; Fernando, I.T.; Kent, K.L. Commutation Failure Analysis in Multi-Infeed HVDC Systems. *IEEE Trans. Power Del.* **2011**, *26*, 378–384. [CrossRef]
28. Chen, X.; Gole, A.M.; Han, M. Analysis of Mixed Inverter/Rectifier Multi-Infeed HVDC Systems. *IEEE Trans. Power Del.* **2012**, *27*, 1565–1573. [CrossRef]
29. Lee, D.H.A.; Andersson, G. An Equivalent Single-Infeed Model of Multi-Infeed HVDC Systems for Voltage and Power Stability Analysis. *IEEE Trans. Power Del.* **2016**, *31*, 303–312. [CrossRef]
30. Aik, D.L.H.; Andersson, G. Power stability analysis of multi-infeed HVDC systems. *IEEE Trans. Power Del.* **1998**, *13*, 923–931. [CrossRef]
31. Aik, D.; Andersson, G. Analysis of Voltage and Power Interactions in Multi-Infeed HVDC Systems. *IEEE Trans. Power Del.* **2013**, *28*, 816–824. [CrossRef]
32. Shao, Y.; Tang, Y. Fast Evaluation of Commutation Failure Risk in Multi-Infeed HVDC Systems. *IEEE Trans. Power Syst.* **2018**, *33*, 646–653. [CrossRef]
33. Merlin, M.M.C.; Green, T.C. Cell capacitor sizing in multilevel converters: cases of the modular multilevel converter and alternate arm converter. *IET Power Electron.* **2015**, *8*, 350–360. [CrossRef]
34. Zhang, Z.; Xu, Z.; Jiang, W.; Bie, X. Operating area for modular multilevel converter based high-voltage direct current systems. *IET Renew. Power Gener.* **2016**, *10*, 776–787. [CrossRef]
35. Kim, H.; Kim, S.; Chung, Y.H.; Yoo, D.W.; Kim, C.K.; Hur, K. Operating Region of Modular Multilevel Converter for HVDC With Controlled Second-Order Harmonic Circulating Current: Elaborating P-Q Capability. *IEEE Trans. Power Del.* **2016**, *31*, 493–502. [CrossRef]
36. Engel, S.P.; Doncker, R.W.D. Control of the Modular Multi-Level Converter for minimized cell capacitance. In Proceedings of the 2011 14th European Conference on Power Electronics and Applications, Birmingham, UK, 30 August–1 September 2011; pp. 1–10.
37. Ilves, K.; Norrga, S.; Harnefors, L.; Nee, H.P. On Energy Storage Requirements in Modular Multilevel Converters. *IEEE Trans. Power Electron.* **2014**, *29*, 77–88. [CrossRef]
38. Guo, C.; Zhang, Y.; Gole, A.M.; Zhao, C. Analysis of Dual-Infeed HVDC With LCC HVDC and VSC HVDC. *IEEE Trans. Power Del.* **2012**, *27*, 1529–1537. [CrossRef]
39. Tang, G.; Xu, Z.; Zhou, Y. Impacts of Three MMC-HVDC Configurations on AC System Stability Under DC Line Faults. *IEEE Trans. Power Syst.* **2014**, *29*, 3030–3040. [CrossRef]
40. Bayo-Salas, A.; Beerten, J.; Rimez, J.; Hertem, D.V. Analysis of control interactions in multi-infeed VSC HVDC connections. *IET Gener. Transm. Distrib.* **2016**, *10*, 1336–1344. [CrossRef]
41. Ni, X.; Gole, A.M.; Zhao, C.; Guo, C. An Improved Measure of AC System Strength for Performance Analysis of Multi-Infeed HVdc Systems Including VSC and LCC Converters. *IEEE Trans. Power Del.* **2018**, *33*, 169–178. [CrossRef]
42. Liu, Y.; Chen, Z. A Flexible Power Control Method of VSC-HVDC Link for the Enhancement of Effective Short-Circuit Ratio in a Hybrid Multi-Infeed HVDC System. *IEEE Trans. Power Syst.* **2013**, *28*, 1568–1581. [CrossRef]
43. Zhou, J.Z.; Gole, A.M. Rationalisation and validation of dc power transfer limits for voltage sourced converter based high voltage DC transmission. *IET Gener. Transm. Distrib.* **2016**, *10*, 1327–1335. [CrossRef]
44. Zygmanowski, M.; Grzesik, B.; Nalepa, R. Capacitance and inductance selection of the modular multilevel converter. In Proceedings of the 15th European Conference on Power Electronics and Applications (EPE), Lille, France, 2–6 September 2013; pp. 1–10. [CrossRef]
45. Tu, Q.; Xu, Z.; Huang, H.; Zhang, J. Parameter design principle of the arm inductor in modular multilevel converter based HVDC. In Proceedings of the 2010 International Conference on Power System Technology, Hangzhou, China, 24–28 October 2010; pp. 1–6. [CrossRef]
46. Gebreel, A.A. Smoothing reactor effect on harmonics and power quality for modular multilevel converter. *Int. J. Sci. Eng. Res.* **2017**, *8*, 78–86.
47. Li, Y.; Jones, E.A.; Wang, F. Circulating Current Suppressing Control's Impact on Arm Inductance Selection for Modular Multilevel Converter. *IEEE J. Emerg. Sel. Top. Power Electron.* **2017**, *5*, 182–188. [CrossRef]
48. Tang, Y.; Ran, L.; Alatise, O.; Mawby, P. Capacitor Selection for Modular Multilevel Converter. *IEEE Trans. Ind Appl.* **2016**, *52*, 3279–3293. [CrossRef]
49. *IEEE Guide for Planning DC Links Terminating at AC Locations Having Low Short-Circuit Capacities*; IEEE: Piscataway, NJ, USA, 1997; pp. 1–216. [CrossRef]
50. Yi, Z. Investigation of Reactive Power Control and Compensation for HVDC Systems. Ph.D. Thesis, University of Manitoba, Winnipeg, MB, Canada, 2011.
51. Franken, B.; Andersson, G. Analysis of HVDC converters connected to weak AC systems. *IEEE Trans. Power Syst.* **1990**, *5*, 235–242. [CrossRef]
52. Wang, F.; Chen, Y. Voltage/Power Stability study upon Power System with Multiple-Infeed Configuration of HVDC Links Using Quasi-Static Modal Anlysis Approach. Master's Thesis, Chalmers University of Technology, Gothenburg, Sweden, 2006.

53. Alstom. *HVDC Connecting to the Future*, 1st ed.; Alstom: Saint-Ouen, France, 2010.
54. *8th Power Supply and Demand Plan for Korean Power System*; Ministry of Trade, Industry and Energy of the Republic of Korea: Sejong, Korea, 2017. Available online: http://www.motie.go.kr/motie/ne/presse/press2/bbs/bbsView.do?bbs_cd_n=81&bbs_seq_n=160040 (accessed on 27 December 2021).
55. *Statistics on Renewable Energy Supply in 2016*; Korea Energy Agency: Gyeonggi-do, Korea, 2017. Available online: https://www.knrec.or.kr/pds/statistics_read.aspx?no=70 (accessed on 27 December 2021).
56. Hur, K. Multi-infeed problems at Jeju HVDC no. 3. In Proceedings of the IEEE Power and Energy Society 2017 Panel Session, Chicago, IL, USA, 16–20 July 2017.